Fatigue Life Predictions for Glassy Polymers: A Constitutive Approach

Roel P. M. Janssen, Dirk de Kanter, Leon E. Govaert,* and Han E. H. Meijer

Materials Technology, Eindhoven University of Technology, P.O. Box 513,
5600 MB, Eindhoven, The Netherlands

Received June 8, 2007; Revised Manuscript Received January 22, 2008

ABSTRACT: Long-term failure under constant or cyclic load is governed by the same process as short-term failure at constant rate of deformation. Failure proves to originate from the polymer's intrinsic deformation behavior, more particularly the true strain softening after yield, which inherently leads to the initiation of localized deformation zones. In a previous study we developed, and validated, a 3D constitutive model that is capable to predict the occurrence of these plastic instabilities, yielding quantitative predictions of the lifetime of polycarbonate under constant load.[1] Here we demonstrate that the same approach is also applicable to predict the life span of polycarbonate under cyclic loading conditions, over a large range of molecular weights and thermal histories, with a single parameter set only. The model incorporates the influence of physical aging, accelerated by the applied cyclic stress. For low cycle fatigue, at large stress amplitudes, where failure is thermally dominated, it is shown that the current constitutive model has to be extended to a multirelaxation time expression to properly describe the (evolution of the) energy dissipation.

I. Introduction

Given their low density as well as low frictional and improved thermal properties,[2–7] engineering polymers provide interesting alternatives for traditional materials, even in load bearing applications. In such applications, the polymer product must be designed to withstand not only high static loads but also cyclic or dynamic fatigue loads, and their design could benefit from the strong computational power available nowadays, employing computer models that describe and predict the polymer's deformation and failure. Costly and time-consuming experiments, now still necessary to assess the fatigue properties of polymers, become redundant. Before discussing all modeling attempts performed so far, we will first deal with the phenomena occurring during the fatigue loading of polymers that are relevant for accurate lifetime predictions.

Fatigue life data are usually presented in an S–N curve, in which the number of cycles (N) that a material can withstand is plotted against the cyclic stress amplitude (S) applied. For thermoplastics, typically two fatigue failure regimes can be distinguished: the so-called low cycle regime, where the material fails after a low number of cycles at high stress, and the high cycle regime at low stress, where the polymer can withstand a large number of cycles before failure. In between we find a transition plateau of a few decades in cycles at a specific changeover stress level. Details can be found in a number of reviews that give a comprehensive overview of all phenomena involved.[8–12]

Characteristic for the *low cycle regime* is that failure is caused by hysteretic heating of the sample, usually leading to ductile failure. Referring to heating as the dominating failure mechanism, this regime is also called the *thermally dominated domain*. Heat generated during fatigue loading cannot be transferred to the surroundings due to the high dissipation in and low thermal conductivity of polymers. For glassy polymers like polycarbonate (PC), poly(methyl methacrylate) (PMMA), and poly(vinyl chloride) (PVC) as well as for semicrystalline polymers like polytetrafluoroethylene (PTFE), polyoxymethylene (POM), and high-density polyethylene (HDPE), it has been shown that thermal failure typically occurs for fatigue signals with a high stress,[13–18] high strain,[19,20] or high frequency.[18–21] Another way of revealing the thermal nature of failure in this regime is by studying hysteresis, since a large and (per cycle) increasing energy dissipation is observed, indicative of failure caused by thermal softening of the polymer.[22–24] To study the (true) fatigue response under isothermal conditions, polymer samples were subjected to fatigue loading under forced convection of air or water[23–26] or, alternatively, the ratio of surface area to volume of the samples was increased to reduce the relative effects of hysteretic heating.[12–16]

The *high cycle regime* can be identified by a high fatigue life due to a low stress applied and/or low frequency. Most often, the failure observed is brittle of nature and only little energy dissipation is found in the hysteresis loops, indicating that the load applied has no significant effect on the temperature of the sample.[22–24] This regime is also referred to as the *mechanically dominated domain*, in which the (true) intrinsic fatigue response can be observed. Particularly in this regime, many studies have found fatigue-induced changes in the mechanical properties of semicrystalline polymers, most often recognized by a decrease in the viscoelastic response.[22–24,27] Opposed to the relatively unknown underlying microstructural rearrangements that play a role in the evolution of mechanical properties of semicrystalline polymers, fatigue-induced changes in glassy polymers appear to be strongly related to the process of physical aging.[28–31] The hypothesis that cyclic stress affects aging kinetics is supported by the fact that, similar to annealing at elevated temperatures, aging kinetics are accelerated by application of stress.[32–35] Moreover, it has been observed that cyclic stress[36,37] causes, similar to constant stress[1] and thermophysical aging,[38–42] an embrittlement of polymers. Despite the similarity in its influence on the macroscopic mechanical behavior, there still is some dispute whether the process of fatigue aging is fully identical to that of physical aging.[44,45]

When trying to predict the fatigue life of engineering polymers, it is important to distinguish the different processes that contribute: crack initiation and crack propagation. In the classical approach to the analysis of fatigue, one concentrates primarily on crack propagation employing fracture mechanics.[46–49] Here it is assumed that a material always contains defects and that the rate-determining step in fatigue failure is

---

* Corresponding author: Tel +31-402472838; Fax +31-402447355; e-mail l.e.govaert@tue.nl.

10.1021/ma071273i CCC: $40.75

the stable growth of such cracks until their size reaches a critical level and failure of the component occurs. Essential in the approach is the dependence of crack growth on the stress intensity amplitude ΔK, which is typically determined in fatigue tests on precracked specimens. An important contribution of fracture mechanics to the engineering practice is that it introduced damage tolerance as an additional safety precaution. Starting point is that a crack becomes detectable before it reaches the critical size.

With respect to the *prediction* of fatigue life, it should be noted that in the fracture mechanics approach the stage of crack initiation is completely neglected. Especially in the case of polymers, however, the initiation stage takes about 95% of the fatigue life.[12] An elegant illustration of the importance of the initiation stage is found in the work of Sauer and Chen,[50] who showed that the crack propagation rate is less for high-impact polystyrene (HIPS) than for polystyrene (PS), whereas fatigue tests on smooth, unnotched samples show that the fatigue life for unmodified PS is appreciably greater than for HIPS. In fatigue tests in uniaxial extension, on smooth samples of PC, polypropylene (PP), and PMMA, we showed that the formation of a crack is preceded by substantial plastic deformation, and the initiation stage almost covers the entire fatigue life (>99%).[51] As a result, quantitative fatigue life estimates are only possible when the initiation stage is included.

Therefore, we now focus on models that deal with on crack initiation rather than crack growth and that indeed proved successful in predicting fatigue life of polymers. They are based on the similarities in deformation and failure kinetics under static (creep) and cyclic loading and focus on predictions of the lifetime under cyclic loading obtained from experimental (static) creep time-to-failure data by using a cumulative damage model.[52–54] Here, it is assumed that failure occurs at a critical amount of damage accumulated as a result of the stress applied according to

$$\int_0^{t_{\mathrm{fail,cyclic}}} \frac{\mathrm{d}t}{t_{\mathrm{fail,static}}[\sigma(t)]} = 1 \qquad (1)$$

where $t_{\mathrm{fail,cyclic}}$ is the time-to-failure as a result of a cyclic stress and $t_{\mathrm{fail,static}}$ is the time-to-failure as a result of a constant stress. The advantage of this route is that the fatigue life can be predicted for any (dynamic) stress history from a set of creep life data. However, this one-dimensional approach does not account for the effect of geometry, and it lacks the ability to account for differences in thermal history and changes in mechanical properties during fatigue as a result of progressive aging.

Recently, Klompen et al.[1] successfully employed a 3D elasto-viscoplastic model to predict the lifetime of the polymer glass PC, loaded at constant stress. In this approach, failure is defined as the onset of a rapid, catastrophic strain localization phenomenon (necking, shear band formation), and therefore it covers only the initiation stage of failure. This proved sufficient for quantitative lifetime predictions for PC in uniaxial extension, planar extension, and shear as well as in more complex geometries under static loading.[55] Apparently, the contribution of stable crack growth to the fatigue lifetime is indeed negligible. The strength of the constitutive model developed is the fact that deformation and failure can be described with a single parameter set, valid *for the total range of molecular weight distributions*. The influence of thermal history is accounted for by only one (state) parameter, S_a, from which the kinetics are captured in a single evolution equation. When the polymer's processing history is known, its value can be computed from the thermal history during cooling to below the glass transition temperature.[56,57] If the history is not known, its present value, S_a, can be determined by applying a simple constant strain rate test to determine the stress at yield. The use of stress activated aging kinetics, leading to accelerated aging during loading, is essential to predict the endurance limit observed in experiments.

Table 1. Number-Averaged and Weight-Averaged Molecular Weights of the PC Grades Used in This Study

grade	M_n [kg/mol]	M_w [kg/mol]
Lexan 141R	9.2	25.8
Lexan 101R	12.7	28.9
extruded rod	14.0	35.9

Rather than following the lines along one of the two categories of research mentioned (fracture mechanics or damage mechanics), in this study we will build on the success of this constitutive approach and investigate the predictive performance of this new line under cyclic, rather than static, stress conditions. First, the model's performance will be evaluated under isothermal conditions. To accomplish this, fatigue testing has been performed on samples with a large surface area to volume ratio under forced cooling in a water tank. Subsequently, fatigue observed under nonisothermal conditions is discussed, and an approach to include its influence in the current model is proposed.

II. Experimental Section

A. Materials. Uniaxial tensile experiments were performed on two different grades of PC (Lexan141R and Lexan101R), provided in the form of granulate by GE Plastics, Bergen op Zoom, The Netherlands. The granulate was dried in an oven at 80 °C for 24 h to prevent degradation during processing. An extrusion grade Lexan (type unknown), supplied as diameter extruded rod, was used for the uniaxial compression tests. Molecular weight distributions are provided in Table 1.

B. Sample Preparation. Isothermal fatigue experiments were performed on thick tensile bars according to ASTM-D638 type IV, injection molded from Lexan101R granulate and cooled at a mold temperature of 30 °C. These will be referred to as *quenched*. To study the influence of thermal history, a group of these samples was *annealed* at 120 °C in an air-circulated oven for 72 h. Nonisothermal experiments were performed on thick tensile bars according to ASTM-D638 type IV, injection molded from Lexan141R granulate. Samples of different thermal history were created by cooling at two different mold temperatures: 30 °C (*quenched*) and 130 °C (*annealed*). Samples for the uniaxial compression tests (ϕ 6 × 6 mm^2) were machined from the extruded rod (Lexan, type unknown). These are referred to as annealed, given the slow cooling inherent to rod extrusion. To create a set of samples with a different thermal history, samples were placed in an oven at 160 °C for 40 min and subsequently *quenched* in ice–water.

C. Mechanical Testing. All mechanical tests were performed on a servo-hydraulic MTS Testing System 810. Prior to testing, samples were allowed to acclimatize for at least 15 min. Tensile tests were performed at constant linear strain rates of 10^{-2}, 10^{-3}, and 10^{-4} s^{-1} in a temperature chamber at 23 °C.

Compression experiments were performed in a temperature chamber at 23 °C under true strain control at constant true strain rates of 10^{-2}, 3×10^{-3}, and 10^{-3} s^{-1} in a compression tool that allowed for accurate alignment. Friction was reduced by applying a thin film of PTFE tape (3M 5480, PTFE skived film tape) onto the sample ends and by lubricating the contact area between steel and tape using a 1:1 mixture of liquid soap and water. During the test no barreling of the sample was observed up to compressive strains of 0.5, indicating that friction was sufficiently reduced.

Fatigue testing was conducted under load control. For each test the maximum stress level of a sine wave was varied, whereas the minimum stress level was kept at 2.2 MPa for all tests (after ref 12). The frequency applied was 2 Hz. For isothermal testing, a special setup was designed to minimize thermal effects from dissipative heating, consisting of a water-filled Plexiglas cylinder mounted on the MTS Testing System, inside which the thick tensile bars were loaded. This cylinder was connected to a circulation bath equipped with a temperature controller and pump, which circulated

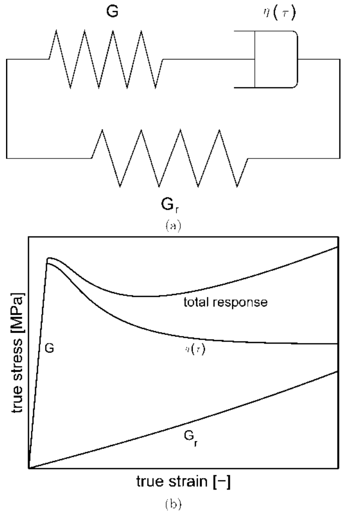

Figure 1. (a) Schematic representation of the employed elasto-viscoplastic model. (b) Schematic representation of the true stress–true strain response of the elasto-viscoplastic model.

water at a temperature of 22 °C into the cylinder. Nonisothermal fatigue testing was performed in an air-circulated temperature chamber at 23 °C. Three types of failure were recognized in fatigue testing (see Figure 4a): stable neck growth, rupture after neck initiation, and brittle fracture. In general, lower load levels induced a more brittle failure mode. In all the different failure modes, the load-applying piston of the testing equipment moves rapidly to the end of its stroke (typically within 3 s). Time-to-failure is defined by the moment that the displacement of the piston was equivalent to a macroscopic strain of 20% (see Figure 4b). In the case of a stable strain localization, a well-developed neck is observed, while for the other cases fracture has already occurred. In compression failure, the strain rapidly increased from –0.1 to –0.8 in 1–2 s. At higher compressive strains the deformation is stabilized by strain hardening.

D. Infrared Thermography. An infrared camera (ThermaCAM PM575, FLIR System AB) was used to quantify heating of the sample during fatigue loading by measuring the temperature distribution. The infrared radiation measured is a function of the emissivity of the material and radiation originating from the surroundings must be compensated for. Therefore, the camera requires the following object parameters: the ambient temperature, the distance between camera and tensile bar, the relative humidity, and the emissivity of the material of the tensile bar. The emissivity of PC was determined by adjusting the emissivity value until the temperature reading of the camera matched that of a thermocouple attached to the tensile bar. An emissivity value of 0.95 was found, which closely matches the value of 0.94 found by Koenen.[58]

III. Constitutive Modeling

In the 3D constitutive models for solid polymers used, the total stress is split into two main contributions, based on the original work of Haward and Thackray:[59]

$$\boldsymbol{\sigma} = \boldsymbol{\sigma}_{\mathrm{s}} + \boldsymbol{\sigma}_{\mathrm{r}} \tag{2}$$

where the driving stress $\boldsymbol{\sigma}_{\mathrm{s}}$ represents the stress contribution of the intermolecular interactions and $\boldsymbol{\sigma}_{\mathrm{r}}$ denotes the strain hardening contribution that is attributed to orientation of the molecular network (see Figure 1 for a schematic representation). The driving stress $\boldsymbol{\sigma}_{\mathrm{s}}$ is split in a deviatoric ($\boldsymbol{\sigma}_{\mathrm{s}}^{\mathrm{d}}$) and a hydrostatic ($\boldsymbol{\sigma}_{\mathrm{s}}^{\mathrm{h}}$) part:

$$\boldsymbol{\sigma}_{\mathrm{s}}^{\mathrm{d}} = G\tilde{\mathbf{B}}_{\mathbf{e}}^{\mathbf{d}} \text{ and } \boldsymbol{\sigma}_{s}^{\mathrm{h}} = \kappa(J-1)\mathbf{I} \tag{3}$$

where G is the shear modulus, $\tilde{\mathbf{B}}_{\mathrm{e}}^{\mathrm{d}}$ the deviatoric part of the isochoric elastic left Cauchy–Green strain tensor, κ the bulk modulus, J the volume change factor, and $\mathbf{I}$ the unity tensor. The evolution of J and $\tilde{\mathbf{B}}_{\mathrm{e}}^{\mathrm{d}}$ is given by the following equations:

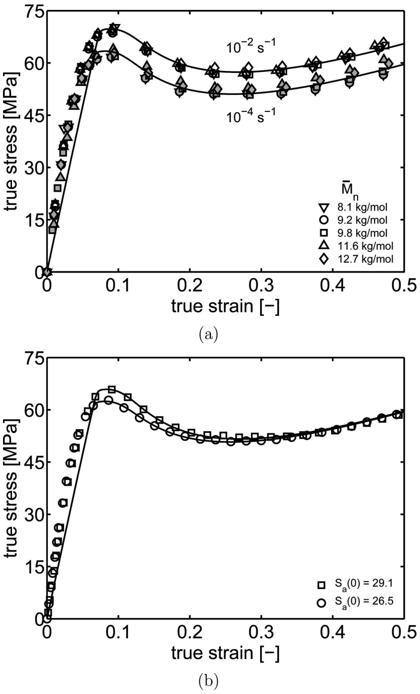

Figure 2. (a) Experimental results (symbols) vs model predictions (lines) of the intrinsic deformation in uniaxial compression at different strain rates for various PC grades. The molecular weight ($\bar{M}_{\mathrm{n}}$) has no influence on deformation. (b) Like (a), now for two different thermal histories. Reproduced with permission from ref 32. Copyright 2005 American Chemical Society.

$$\dot{J} = J\,\mathrm{tr}(\mathbf{D}) \tag{4}$$

$$\overset{\circ}{\tilde{\mathbf{B}}}_{\mathrm{e}} = (\mathbf{D}^{\mathrm{d}} - \mathbf{D}_{\mathrm{p}})\cdot\tilde{\mathbf{B}}_{\mathrm{e}} + \tilde{\mathbf{B}}_{\mathrm{e}}\cdot(\mathbf{D}^{\mathrm{d}} - \mathbf{D}_{\mathrm{p}}) \tag{5}$$

where $\overset{\circ}{\tilde{\mathbf{B}}}_{\mathrm{e}}$ is the Jaumann derivative of $\tilde{\mathbf{B}}_{\mathrm{e}}$ and $\mathbf{D}^{\mathrm{d}}$ the deviatoric part of the rate of deformation tensor. The plastic part of the rate of deformation tensor $\mathbf{D}_{\mathrm{p}}$ is given by

$$\mathbf{D}_{\mathrm{p}} = \frac{\boldsymbol{\sigma}_{\mathrm{s}}^{\mathrm{d}}}{2\eta T, \bar{\tau}p, S)} \tag{6}$$

Under isothermal conditions the nonlinearity of the model is completely governed by a stress, pressure, and state dependent viscosity function η, defined as[32]

$$\eta(T,\bar{\tau},p,S) = \eta_{0,r}(T)\cdot\underbrace{\frac{\bar{\tau}/\tau_0}{\sinh(\bar{\tau}/\tau_0)}}_{\text{(I)}}\cdot\underbrace{\exp\left(\frac{\mu p}{\tau_0}\right)}_{\text{(II)}}\cdot\underbrace{\exp\left(S(t,\bar{\gamma}_p)\right)}_{\text{(III)}} \tag{7}$$

with $\eta_{0,\mathrm{r}}(T)$ the zero viscosity for the completely rejuvenated state and the equivalent stress. The stress dependence of the viscosity is governed by the parameter τ_0, the pressure dependence by the parameter μ, while p is the hydrostatic pressure. Together, the parts marked (I) and (II) represent the pressure modified Eyring flow equation as originally proposed by Duckett et al.[60] Part (III) describes the dependence of the viscosity on the material state expressed by the state parameter S.

The material state S is determined by two processes: physical aging, measured as an increase in yield stress, and mechanical rejuvenation during loading, measured as true strain softening.[32] In the model, these two processes are decoupled: $S(t,\bar{\gamma}_{\mathrm{p}}) = S_{\mathrm{a}}(t)R_{\gamma}(\bar{\gamma}_{\mathrm{p}})$. In this expression, the function R_{γ} describes the

Table 2. Material Parameters for PC at a Reference Temperature of 23 °C (Reproduced from Ref 32)

E [MPa]	900	r_2	−5
ν	0.4	G_r [MPa]	26
$\eta_{0,r}$ [MPa·s]	2.1×10^{11}	c_0	−4.41
τ_0 [MPa]	0.7	c_1	3.3
μ	0.08	t_a [s]	−
S_a	−	ΔU_a [kJ/mol/K]	205
r_0	0.965	$\bar{v}_a$ [m³/mol]	1.33×10^{-3}
r_1	50		

mechanical rejuvenation upon plastic deformation $\bar{\gamma}_p$ and is given by a modified Carreau−Yasuda expression:[61]

$$R_\gamma(\bar{\gamma}_p) = \frac{(1 + (r_0 \exp(\bar{\gamma}_p))^{r_1})^{(r_2-1)/r_1}}{(1 + r_0^{\,r_1})^{(r_2-1)/r_1}} \tag{8}$$

where $\bar{\gamma}_p$ denotes the equivalent plastic strain, and r_0, r_1, and r_2 are fitting parameters. The aging contribution is $S_a(t)$:

$$S_a(t_{\text{eff}}) = c_0 + c_1 \log\left(\frac{t_{\text{eff}}(t,\ T, \bar{\tau}) + t_a}{t_0}\right) \tag{9}$$

where $t_0 = 1$ s, c_0 and c_1 are constants, t_a is the initial age, and t_{eff} is the effective time, defined as

$$t_{\text{eff}}(t,\ \bar{\tau}, T) = \int_0^t \frac{d\xi}{a_\sigma(\bar{\tau}(\xi))a_T(T(\xi))} \tag{10}$$

where a_σ is a stress activation of the Eyring type and a_T is a temperature shift function of the Arrhenius type

$$a_\sigma(\bar{\tau}(t)) = \frac{\bar{\tau}(t)/\tau_a}{\sinh(\bar{\tau}(t)/\tau_a)} \quad \text{with } \tau_a = \frac{RT}{\bar{v}_a} \tag{11}$$

$$a_T(T(t)) = \exp\left(\frac{\Delta U_a}{R}\left(\frac{1}{T} - \frac{1}{T_{\text{ref}}}\right)\right) \tag{12}$$

where $\bar{v}_a$ denotes the activation volume for aging, ΔU_a the activation energy, R the universal gas constant, and T the absolute temperature. T_{ref} is the temperature at which the temperature-dependent aging is characterized.

Strain hardening is, finally, modeled with a single neo-Hookean spring:

$$\boldsymbol{\sigma}_r = G_r\tilde{\mathbf{B}}^d \tag{13}$$

where G_r is the strain hardening modulus and $\tilde{\mathbf{B}}^d$ the deviatoric part of the isochoric left Cauchy−Green deformation tensor.

A comparison between the model's predictions, using the parameter set in Table 2, and the experimental results under (short-term) uniaxial compression testing is illustrated in Figure 2. The strain rate dependence of yield and postyield behavior of a wide range of commercially available PC grades is captured well by the model (Figure 2a). Apparently, there is *no influence of molecular weight distribution* on the deformation kinetics. This can be rationalized by the fact that the deformation in the glassy state is controlled by intermolecular interactions. Since these act on a segmental scale, the role of chain length is expected to be minor. The description of strain softening is accurate for different thermal histories by adjusting only the state parameter S_a (Figure 2b). Moreover, the model also provides excellent time-to-failure predictions under (long-term) constant stress loading as shown in Figure 3a. Essential for the, indeed measured and predicted, endurance limit (stress below which no failure occurs) is the implementation of the stress-induced aging kinetics that leads to an increase of the state parameter S in time (eq 9) (see Figure 3b). As a result, the rate of development of plastic deformation decreases, which gives rise to the endurance limit observed.[1]

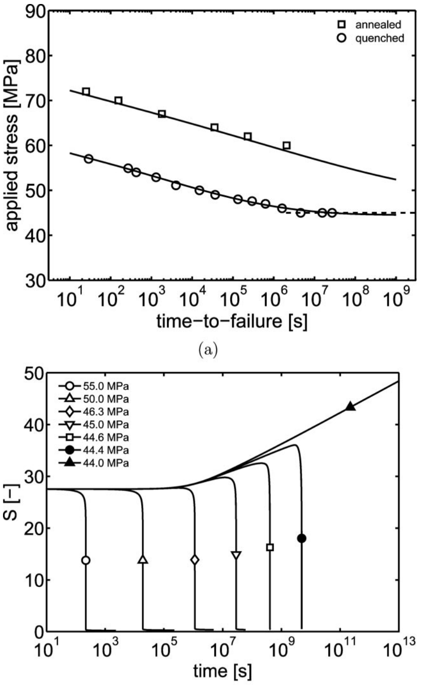

(a)

(b)

Figure 3. (a) Experimental results (symbols) vs numerical predictions (lines) of the lifetime of PC under static loading. Aging kinetics are included in the model. (b) Evolution of the state parameter S as a function of time for quenched PC at different stress levels. Reproduced from ref 1. Copyright 2005 American Chemical Society.

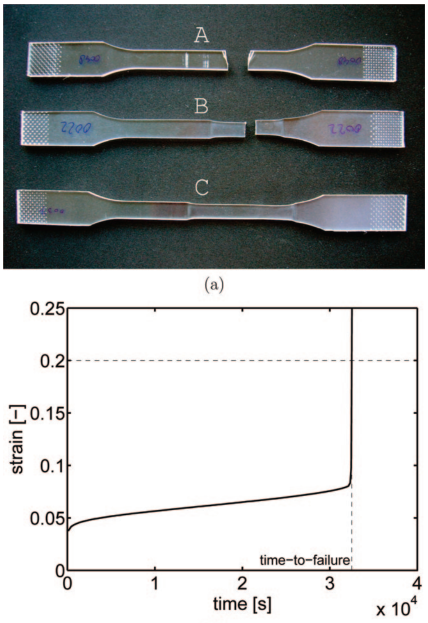

(a)

(b)

Figure 4. (a) Macroscopic failure behaviour of PC at different loads. All samples were quenched and tested in nonisothermal conditions (results presented in Figure 9a). A: fracture (maximum stress of 56 MPa); B: rupture after neck initiation (maximum stress of 58 MPa); C: stable neck growth (maximum stress of 61 MPa). (b) Experimental time-to-failure of PC under stress loading (55 MPa) is determined at a macroscopic strain of 20%.

Additional results based on (short-term) tension experiments concerning the pressure dependence of the yield stress, aging kinetics, and molecular weight dependence are given elsewhere.[32] The resulting relevant material parameters are reproduced in Table 2. Values for the parameter S_a, the initial value

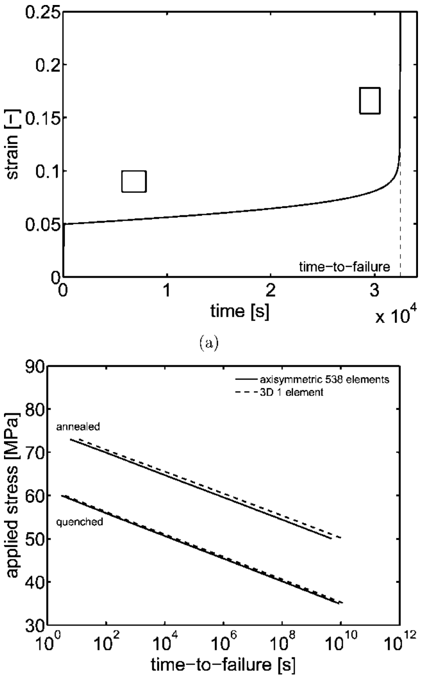

(a)

(b)

Figure 5. (a) Single-element simulation of stress loading (55 MPa) with an S_a of 31.5, similar to the experiments. The numerical time-to-failure is also determined at a macroscopic strain of 20%. (b) No substantial difference is found in predicted times-to-failure between the notched axisymmetric model of 537 elements used by ref 1 (solid lines) and a (unnotched) single analysis (dashed lines). Both methods predict the experimental lifetime accurately (not shown here).

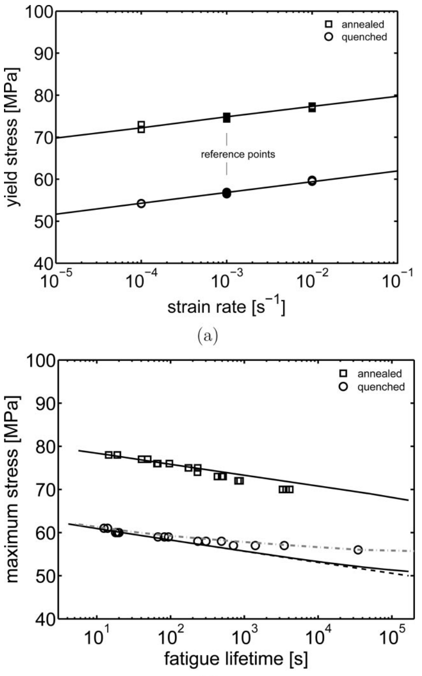

(a)

(b)

Figure 6. (a) Yield stress (engineering) vs strain rate and (b) fatigue lifetime for quenched and annealed PC (Lexan101R) in uniaxial tension under isothermal conditions. The experimental results are represented by symbols; the lines represent model predictions excluding (dashed) and including (solid) aging kinetics. In the case of annealed PC the predictions with and without aging are identical (within the time-range plotted), and hence both lines (dashed and solid) are exactly on top of one another. The gray dash-dot line represents predictions using the actual aging kinetics experimentally observed in fatigue (see Figure 7b).

for S at the initial age t_a, are not provided since they are determined for each material separately measuring the yield stress at a single strain rate.

IV. Numerical Simulations

In the simulations an axisymmetric model of a tensile bar with a small imperfection in the middle was used.[1,42] The mesh consisted of 537 8-node second-order elements. This cylindrical tensile bar has a parallel length of 1 and a radius of 0.2. The circular imperfection has a radius of 0.02 and a maximum depth of 0.003, being 1.5% of the bar's radius and acts as an initiation site for strain localization. Govaert et al.[43] showed that size and shape of the imperfection have a minor influence on the deformation of the tensile bar as only the draw ratio during stable neck growth is slightly affected. An adaptive time stepping method was employed to perform (long-term) creep simulations,[1] and the time step is adjusted according to a prescribed critical strain increment. Such a method significantly reduces the calculation times of (long-term) creep simulations in comparison with constant time stepping protocols. However, it is self-evident that for cyclic loading the advantage of adaptive time stepping cannot be exploited. Moreover, a time step of around 0.01 is required, which equals 50 steps per cycle, to properly describe the prescribed sinusoidal fatigue signal. As a result, large computing times can be expected to model fatigue loading at low stresses, where the observed lifetimes are in the order of 10^5 s. To reduce simulation times, an investigation to the influence of mesh size on predicted times-to-failure under (uniaxial) creep loading is carried out first. The extreme case of only a single is compared to a fully meshed axisymmetric bar.[1] Failure in the simulation is, similar to that in the experiments, defined at the moment at which a macroscopic strain of 20% is reached (see Figure 4b (experiment) and Figure 5a (simulation)). Please note that failure in the simulations is always ductile, since the transition from ductile to brittle is determined by reaching a critical hydrostatic stress,[70] which is not accounted for, yet, in the model. From Figure 5b, it is concluded that there is no significant difference between the predicted time-to-failure in simulations using either the tensile bar model or the single element model. This small difference is likely to be related to the imperfection. For practical reasons only, in this study a single is used to perform lifetime predictions under cyclic loading.

V. Results

A. Isothermal Fatigue. The large energy dissipation and low thermal conductivity of thermoplastics cause catastrophic thermal failure during cyclic fatigue at high stress, high strain, or high frequency.[13–22] Thus, we can only try to measure the (true) *mechanical* fatigue response if we suppress the nonisothermal effects caused by dissipative heating.[13–16,23–26] To achieve this, samples with a large surface area to volume ratio were loaded under forced water cooling. Two sets of samples with different thermal histories (*quenched and annealed*) were prepared. First, the results of *tensile* fatigue are discussed, followed by those obtained during fatigue testing under *compression*.

Differences in the initial state of the polymer as a result of a different thermal history have a profound effect on the yield stress (see Figure 6a), while the strain-rate dependence, i.e. the slope of yield stress vs the logarithm of strain rate, remains unchanged. These observations are consistent with results reported in the literature.[1,62–64]

Loading the samples in fatigue tests, using a sinusoidal stress function varying between the minimum stress of 2.2 MPa and different maximum stresses (see Figure 6b), shows that annealed

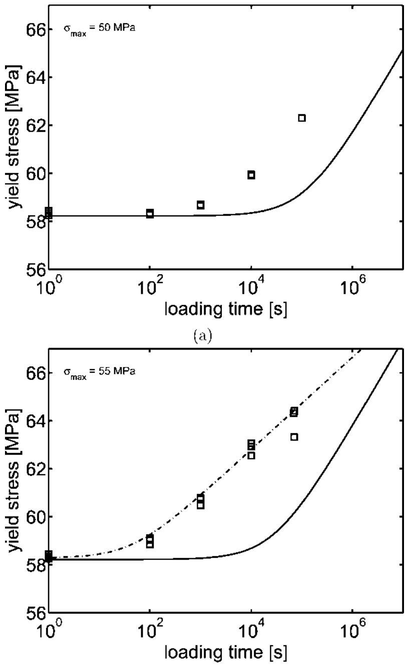

(a)

(b)

Figure 7. Evolution of yield stress as a function of loading time at for quenched PC (Lexan101R) subjected to a cyclic stress in tension with a maximum value of (a) 50 MPa and (b) 55 MPa. The symbols represent the experiments; the solid lines the model predictions using the parameters listed in Table 2. The dash-dot line is obtained by adapting the parameters and governing the aging kinetics (eq 9).

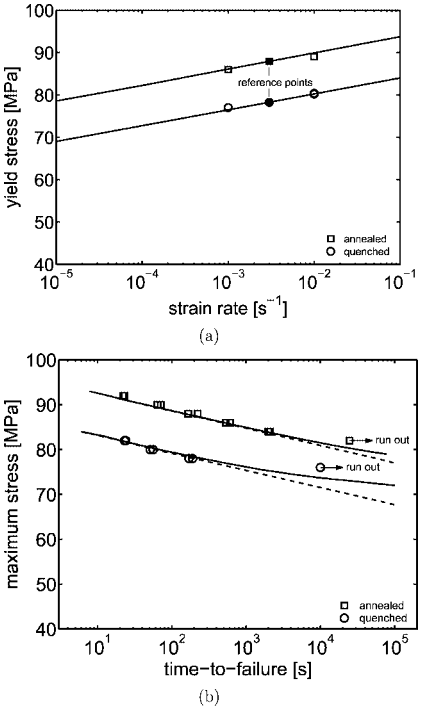

(a)

(b)

Figure 8. (a) Yield stress (engineering) vs strain rate and (b) fatigue lifetime of quenched and annealed PC (Lexan: extruded rod) in uniaxial compression under isothermal conditions. The experimental results are represented by symbols; the lines represent model predictions excluding (dashed) and including (solid) aging kinetics.

samples can withstand a much higher maximum stress for a given time-to-failure than quenched samples, which is in complete analogy with findings of Klompen et al., who tested this polymer under constant stress (static fatigue).[1] In contrast with curves obtained under nonisothermal conditions,[12,16] we find no plateau in the lifetime curves. The absence of two different domains (a *thermal and a mechanical*, see below) is a strong indication that the measures applied to suppress the effects of hysteretic heating were effective. All samples loaded in tension and fatigue exhibit ductile failure, i.e. neck formation.

In order to predict lifetimes using the constitutive model described, it is necessary to determine the state parameter S_a to account for differences in the initial material state at age t_a. S_a is fitted to the (engineering) yield stress data obtained at a strain rate of 10^{-3} s^{-1} (see the reference points in Figure 6a), and values of 27.3 and 43.6 are found for the quenched and annealed samples, respectively. Using these values of S_a, we find an accurate description of the strain rate dependence of the yield stress for the two thermal histories (solid lines in Figure 6a). The simulations were made (1)without stress-accelerated physical aging, in which case the S_a value was kept constant during the simulation, and (2) with stress-accelerated physical aging, in which case the S_a value was allowed to evolve during the simulation (captured by eq 9). In the latter case the S_a value is replaced by the initial age t_a, being 4×10^9 s for the quenched and 3.5×10^{14} s for the annealed material. The solid and dashed lines in Figure 6b are the lifetime predictions of the model under cyclic loading with and without stress-induced aging taken into account, respectively. Quantitatively accurate lifetime predictions are found for the annealed samples, while for the quenched samples we find good predictions at high stress levels, whereas at low stresses, where an endurance limit seems to appear, a deviation is observed. Klompen et al.[1] showed for constant stress loading that stress-induced aging kinetics are the cause of the endurance limit observed (see Figure 3) and produced quantitative predictions. The change in slope in Figure 6b is clearly not predicted when progressive physical aging during fatigue is taken into account (the solid line in Figure 6b).

To test its cause, samples were fatigued at a maximum stress 50 and 55 MPa for 10^2, 10^3, 10^4, and 10^5 s. Subsequently, a tensile test was performed at 10^{-3} s^{-1} to study the evolution of the yield stress. The experimental results (symbols in Figure 7) show, after an initial plateau, a significant increase in yield stress as a result of the cyclic stress applied. Apparently, the cyclic stress loading, similar to constant stress loading,[32] accelerates physical aging. This observation is in full accordance with other literature data.[28–31,36,44,45]

To quantitatively compare aging kinetics observed in static and dynamic loading, we now apply the evolution kinetics found by Klompen et al. in static loading conditions[32] to predict the yield stress development in cyclic loading (Figure 7), accomplished by using a stress-dependent effective time, t_{eff}, based on the shift factor a_σ, shown in eq 9, to describe the evolution of yield stress during fatigue loading. The equivalent stress applied $\bar{\tau}(t)$ is given by

$$\bar{\tau}(t) = \bar{\tau}_{mean} + \bar{\tau}_{ampl} \sin(2\pi f t) \tag{14}$$

where $\bar{\tau}_{mean}$ is the equivalent mean stress, $\bar{\tau}_{ampl}$ is the equivalent stress amplitude, f is the frequency, and t is the elapsed time. Combination of eqs 10, 14, and 9 yields the evolution of the state parameter S_a during fatigue, applying the aging parameters as given in Table 2. Yield stresses were subsequently calculated for various loading times using single element FEM simulations, with the appropriate S_a value, of uniaxial tensile tests at a constant strain rate of 10^{-3} s^{-1}. The result, presented by the solid lines in Figure 7, indicates that the evolution of yield stress observed during fatigue is much faster than that predicted by the model of Klompen et al.[32] This result is in accordance with the poor prediction of the onset of the endurance limit found in Figure 6b. A possible explanation for this discrepancy might be the difference in stresses applied by Klompen et al. to characterize the stress-dependent aging

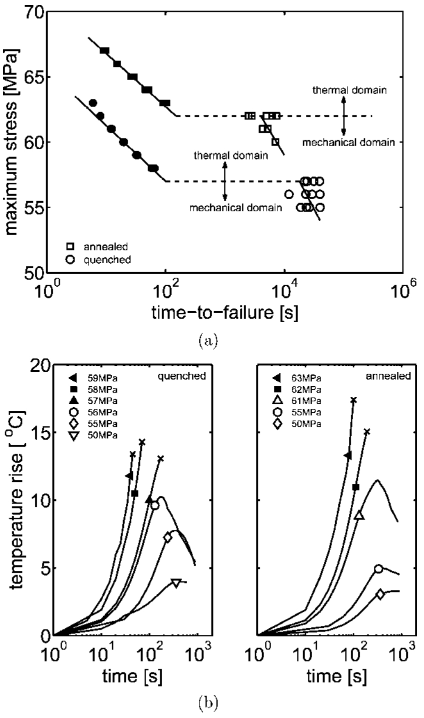

Figure 9. (a) Fatigue lifetime of quenched and annealed PC (Lexan141R) in uniaxial tension under nonisothermal conditions. (b) Temperature increase during fatigue for quenched (left) and annealed (right) PC (Lexan141R). The solid symbols represent the thermal domain, whereas the mechanical domain is represented by the open symbols. The lines are a guide to the eye.

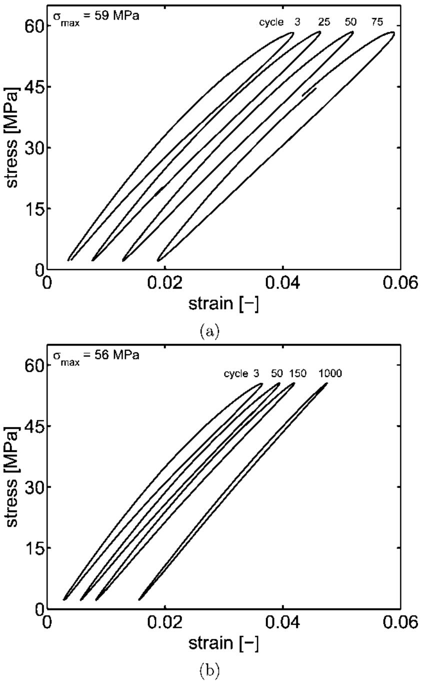

Figure 10. (a) Thermal domain: hysteresis loops of quenched PC (Lexan141R) subjected to a cyclic load with a maximum stress of 59 MPa. (b) Mechanical domain: the maximum stress equal to 56 MPa.

kinetics (0, 13, and 26 MPa at 80 °C[32]) and the stresses applied in our fatigue experiments (up to 60 MPa at 23 °C). Apparently, stress activation is much stronger at elevated stress levels. Most important, however, is that the results clearly indicate that stress-accelerated aging occurs during fatigue loading.

To demonstrate that the onset of the endurance limit, observed for the quenched samples in Figure 6b, is directly related to the stress-activated evolution of the yield stress, we fitted the parameters governing aging kinetics (described by eq 9) to the experimentally observed increase in yield stress during cyclic loading with a maximum stress of 55 MPa (dash-dot line in Figure 7b). In the fitting procedure the stress activation was not changed, and the resulting values of the aging parameters were $c_0 = 14.57$ and $c_1 = 1.76$, leading to a new value of $t_a = 1.7 \times 10^7$. With this improved description we again simulated the fatigue life for the quenched samples (see the gray dash-dot line in Figure 6b) and now find excellent agreement with the experimental data. This clearly illustrates that also for cyclic fatigue the onset of an endurance limit is directly related to the evolution of the yield stress.

Figure 8a shows the strain rate dependent yield stress of the annealed and quenched extruded rod in uniaxial compression. In Figure 8b, the fatigue life of these samples under *compressive* loading is shown. The first conclusion is that for the same time-to-failure in compression the stresses applied can be higher than in *tension* (Figure 6a), again showing high values for the annealed samples. Second, also in compression the observed failure is ductile, which is recognized by bulging of the sample. To perform the simulations, the initial age S_a of the material was determined: 29.5 for the quenched and 35.7 for the annealed samples. Strain rate dependent yield in compression is predicted well (see Figure 8a), as are the fatigue lifetime predictions (see Figure 8b). Without aging kinetics (dotted lines) the model gives accurate lifetime predictions in *compression* at high stress only and again fails to predict the endurance limit observed at lower stress, like for the tensile fatigue results in Figure 6b. Including aging kinetics, the predictions (solid lines) show an earlier onset to the endurance limit than observed in tensile. Also here, however, the onset occurs later than experimentally observed.

It is stressed that the PC grades used in tensile and compression have different molecular weight distributions (see Table 1). Despite this difference, the model provides accurate lifetime predictions for both grades.

B. Nonisothermal Fatigue: Observations. Having confidence in the results achieved in the rather artificial isothermal fatigue tests, we now consider the situation where self-heating of polymers is allowed. The lifetime curves, resulting from testing a large number of PC samples in nonisothermal conditions, are summarized in Figure 9a. Two failure domains can be distinguished: a *thermal and a mechanical* domain with a transition at a specific stress: 56 MPa for quenched and 61 MPa for annealed samples. An infrared camera was used to record heating in both domains (see Figure 9b).

If the maximum stress is larger than a critical stress (filled symbols), the temperature increases continuously until failure occurs. Heating plays a key role in failure in this so-called *thermal domain*. In the *mechanical* domain (open symbols), the temperature shows an initial rise followed by a decrease, indicating that failure is not thermally dominated. Above the changeover stress, samples fail ductile via neck formation, whereas below this changeover stress, brittle fracture is observed. Observations in literature on heating[13−18] and failure[15,16,22] are fully consistent with our findings.

Figure 10a shows the hysteresis loops of quenched PC loaded in the *thermal domain* ($\sigma_{max} = 59$ MPa). The increase in area in the hysteresis loops indicate a substantial energy dissipation, in agreement with the observations on the continuously increasing temperature in this domain (Figure 9b). Figure 10b shows loops in the mechanical domain ($\sigma_{max} = 59$ MPa), where a continuous decrease in hysteresis is observed, which is in full accordance with the observed decrease in surface temperature in Figure 9b. Similar observations were made on polyacetal by Lesser.[22]

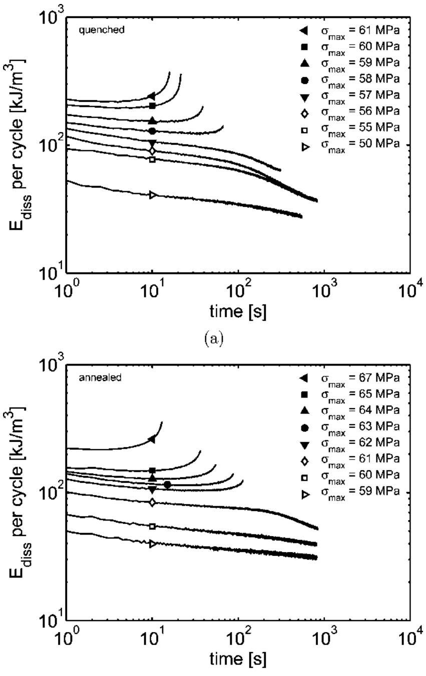

(a)

(b)

Figure 11. (a) Energy dissipation per cycle vs time for quenched PC (Lexan141R). (b) Same as (a), now for annealed PC (Lexan141R). The filled symbols represent the thermal domain and open symbols the mechanical domain.

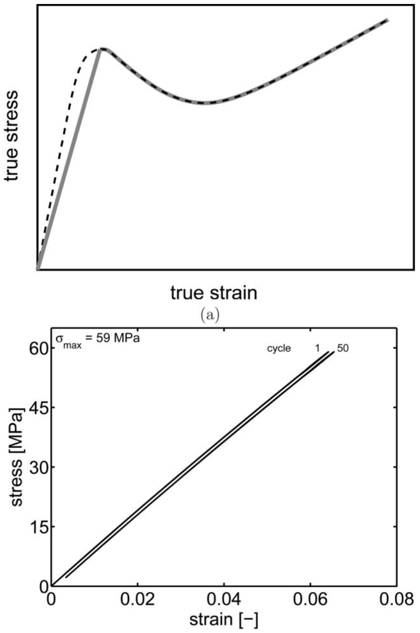

(a)

(b)

Figure 12. (a) Schematic representation of the intrinsic deformation of glassy polymers as obtained from experiments (dashed line) and the current single-mode model (solid line). (b) Prediction of the hysteresis loops for a cyclic signal with at maximum stress of 59 MPa (thermal domain) by the current single-mode model.

The energy dissipation per cycle is shown in Figure 11. In the *thermal domain* (filled symbols) the energy dissipation is large, but a slight decrease is observed from the start of the experiment, which is followed by an abrupt and rapid increase. For an interpretation of these findings, we refer to Figure 3b which shows, by means of the state parameter S, that the lifetime of PC is determined by strain softening, recognized by the strong decrease of S, but can be prolonged by physical aging, which results in an increase of S.

Since physical aging induces an increase in stiffness, it can be expected that it causes the small initial decrease in energy dissipation, which is in line with observations that physical aging causes a decrease in loss angle tan(δ) during loading.[39,44,65–69] However, with ongoing loading, an itself accelerating effect can be anticipated that explains the rapid increase in energy dissipation just before failure and overrules the effect of physical aging: due to the large initial energy dissipation, the sample temperature rises (Figure 9b), which causes a decrease in stiffness of the material that in turn results in a larger hysteresis and energy dissipation. In the *mechanical domain* (open symbols) a continuous decrease in dissipated energy is observed, with a remarkable change in slope after 100 s. The latter is an indication that from this point on the competition between (thermal) softening and physical aging is solely controlled by aging, which is corroborated by the sudden decrease in temperature in the mechanical domain at this time scale (see Figure 9b). In addition, fatigue-induced aging explains the slight increase in stiffness observed in the hysteresis loops in Figure 10b and confirms the embrittlement in the mechanical domain.[38–42]

C. Nonisothermal Fatigue: Thermomechanically Coupled Modeling.

The nonisothermal experiments show a substantial effect of hysteretic heating on the lifetime of glassy polymers at high stresses. Therefore, thermomechanical simulations are required to acquire accurate lifetime predictions in this loading range. Heating is caused by energy dissipation

$$\Delta T_{\text{cycle}} = \frac{\Delta Q_T}{c_p \rho} \tag{15}$$

where $\Delta T_{\text{cycle}}$is the temperature increase per cycle, ΔQ_T is the thermal part of the dissipated energy per unit volume per cycle, ρ is the density of the polymer, and c_p is the specific heat. Rittel and Rabin[71] found good agreement between experimentally observed temperatures and numerical predictions, using the experimentally dissipated energy, measured from the area enclosed by a hysteresis loop, as an input and by taking heat losses to the surroundings into account. Hence, in order to perform thermomechanically coupled lifetime predictions, it is essential that the constitutive model employed provides an accurate description of the energy dissipation.

The constitutive models used up to now are especially designed to accurately capture the postyield behavior, and therefore the use of a one mode Maxwell element only causes the preyield response to be only approximate (see Figure 12a). Predictions of this model for the hysteresis loops of cycle 1 and cycle 50 in the thermal domain ($\sigma_{\text{max}} = 59$ MPa) are plotted in Figure 12b, and as expected no energy is dissipated according to this linear elastic single mode preyield description. This result is not surprising, since it is well-established that the viscoelastic properties of polymers (neglected in this elastic-up-to-yield approach) cause the hysteresis.

An adequate description of the material's behavior is obtained using a model describing (only) the nonlinear viscoelastic behavior of PC up to yield, adopted from ref 72 (see Figure 13a). To predict the hysteresis loops from the prescribed stress signal

$$\sigma(t) = \sigma_{\text{mean}} + \sigma_{\text{ampl}} \sin(2\pi f t) \tag{16}$$

a Boltzmann single integral representation in strain formulation in combination with a stress reduced time is used:

$$\epsilon(t) = \int_0^t D(\psi - \psi')\dot{\sigma}(t')\,\mathrm{d}t' \tag{17}$$

with

$$\psi = \int_0^t \frac{\mathrm{d}t''}{a_\sigma[\sigma(t'')]} \text{ and } \psi' = \int_0^{t'} \frac{\mathrm{d}t''}{a_\sigma[\sigma(t'')]} \tag{18}$$

$$a_\sigma = \frac{\sigma/\sigma_0}{\sinh(\sigma/\sigma_0)} \text{ with } \sigma_0 = \frac{kT}{\nu} \tag{19}$$

where k is Boltzmann's constant, T is the absolute temperature, and v represents the activation volume. For an n-mode sequential Kelvin–Voigt model, $D(t)$ reads

$$D(t) = D_0 + \sum_{i=1}^{n} D_i\left[1 - \exp\left(-\frac{t}{\tau_i}\right)\right] + \frac{t}{\eta_0} \tag{20}$$

where D_0 represents the initial elastic response, η_0 is the flow viscosity, D_i and T_i are the compliance and retardation time of the ith Kelvin–Voigt element, and n represents the number of elements. The samples used in our study have a different thermal history and consequently a different yield stress, which should be corrected for. Therefore, the retardation time spectrum τ'_i and flow viscosity η'_0 adopted from ref 72 are shifted as follows:

$$\tau_i = \tau'_i \exp(\Delta S_\mathrm{a}) \text{ and } \eta_0 = \eta'_0 \exp(\Delta S_\mathrm{a}) \tag{21}$$

with ΔS_a the difference in the state parameter S_a between samples used in this work and those in ref 72. The original and shifted retardation time spectra are tabulated in the Appendix. Comparing the results, Figure 13b, to the experimentally obtained hysteresis loops, Figure 10a, it is clear that the multimode approach gives a much more realistic description of the energy dissipation during cyclic loading than the single mode approach (see Figure 12).

The predicted hysteresis loops are used to quantify the energy dissipation, from which the temperature increase is determined using eq 15. ΔQ_T in this equation is usually only part of the total work dissipated ΔQ:

$$\Delta Q_T = \beta \Delta Q \tag{22}$$

where β has a value in the range of 0.5–1.[73–76] Rittel and Rabin[71] performed simulations to predict the temperature increase during cyclic loading and used a β value of 0.5. Here we will use values for β in the range $0.5 \leq \beta \leq 1$. Only the average heating rate during the first is considered, since changes due to heating, to plastic deformation, or to physical aging in the shape of the hysteresis loops are not accounted for in the model. Figure 14 compares the experimental initial heating rate (symbols) of quenched (a) and annealed (b) PC to values predicted for single mode (dotted lines) and multimode models (solid lines) as a function of the maximum stress applied during loading. Again, it is confirmed that the current single-mode approach cannot account for hysteretic heating, but it is clearly shown that the multimode version accurately describes the experimental results for both quenched and annealed PC. From this example, we can conclude that a modification of the current single-mode approximation used in the most advanced constitutive modeling of solid polymers into a multimode description of the (visco-elastic) deformation behavior up to yield is a prerequisite to perform quantitative thermomechanically coupled simulations. Therefore, no attempt is made yet to predict the lifetime of PC under nonisothermal conditions shown in Figure 9a. This will be postponed until the multimode version is fully developed and implemented.[77]

D. Influence of Aging on the Ductile-to-Brittle Transition. Under nonisothermal conditions two failure domains were distinguished: a thermally dominated domain, where ductile failure is observed, and a (isothermal) mechanically dominated failure domain, where the samples fracture brittle. This rather sharp transition in failure mode can be explained by observations in each of the domains: in the thermal domain, the samples showed a continuous increase in temperature, which promotes ductile failure, while physical aging, recognized by an increase in yield stress and a decrease in loss angle, appears to play a key role in the brittle fracture observed in the mechanical

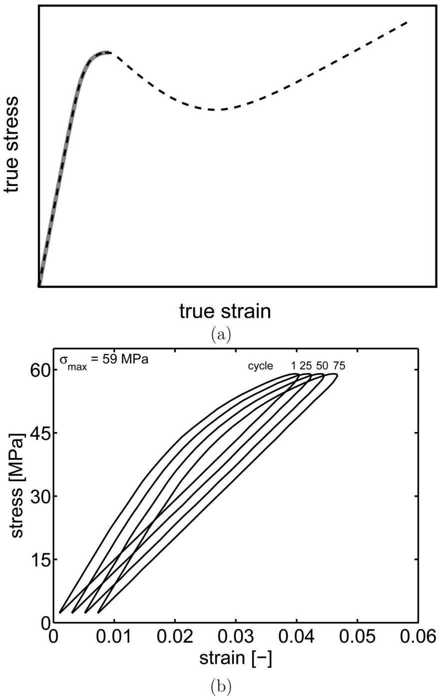

Figure 13. (a) Schematic representation of the intrinsic deformation of glassy polymers as obtained from experiments (dashed line) and a multimode modeling approach (solid line). (b) Prediction of the hysteresis loops for a cyclic signal with at maximum stress of 59 MPa (thermal domain) by the multimode model.

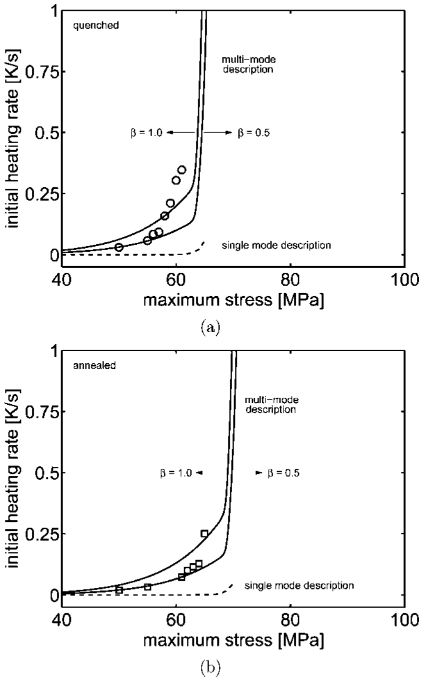

Figure 14. Comparison of predicted heating rate during cyclic loading by the single-mode (dashed line) and multimode model (solid line) to experimental results (symbols) for (a) quenched and (b) annealed PC (Lexan141R).

Table 3. Retardation Times Determined from Lexan 161R at 23 °C, with a S_a Value of 28.3[72]

i	$\tau_{i,0}$ [s]	D_i [GPa^{-1}]
1	3.14×10^3	0.00878
2	3.59×10^4	0.00485
3	4.10×10^5	0.00524
4	4.68×10^6	0.00470
5	5.34×10^7	0.01283
6	6.10×10^8	0.01634
7	6.97×10^9	0.02057
8	7.96×10^{10}	0.02559
9	9.09×10^{11}	0.03076
10	1.04×10^{13}	0.04076
11	1.19×10^{14}	0.04839
12	1.35×10^{15}	0.06606
13	1.55×10^{16}	0.09883
14	1.77×10^{17}	0.04723

$D_0 = 0.419$ [GPa^{-1}]

$\eta_0 = 2.74 \times 10^{21}$ [MPa·s]

Table 4. Shifted Retardation Times Used for Lexan 101R at 23 °C, with a S_a Value of 29.5

i	T_i	D_i [GPa^{-1}]
1	1.04×10^4	0.00878
2	1.19×10^5	0.00485
3	1.36×10^6	0.00524
4	1.55×10^7	0.00470
5	1.77×10^8	0.01283
6	2.02×10^9	0.01634
7	2.31×10^{10}	0.02057
8	2.64×10^{11}	0.02559
9	3.02×10^{12}	0.03076
10	3.45×10^{13}	0.04076
11	3.95×10^{14}	0.04839
12	4.48×10^{15}	0.06606
13	5.15×10^{16}	0.09883
14	5.88×10^{17}	0.04723

$D_0 = 0.419$ [GPa^{-1}]

$\eta_0 = 9.10 \times 10^{21}$ [MPa·s]

domain, which is in agreement with reports of embrittlement of glassy polymers upon thermophysical aging[38–42] or stress-accelerated aging.[1] Since failure of all samples in the isothermal experiments was also ductile, we conclude that physical aging, rather than hysteretic heating, is the dominating process that affects the time scale at which the ductile-to-brittle transition occurs in fatigue testing. Since the aging kinetics strongly depend on the initial age of the polymer, the thermomechanical history is expected to have great influence on the time scale of the transition.

The origin of the ductile-to-brittle transition can be explained by a change of the intrinsic deformation behavior of the polymer,[1,42] which after yielding shows strain softening, a decrease in true stress upon deformation that erases the prior thermal history, followed by strain hardening. Strain softening is triggered by stress concentrations that originate from inhomogeneities and leads to a localized development of plastic strain, which, with ongoing deformation, is stabilized by strain hardening, and a stable neck will propagate. Upon aging, either prior to[1,42] or during testing (here), yield stress and strain softening increase, which enhances the localization of strain and thus the local true stress, while the strain hardening remains unaffected (see Figure 2b). When this (local) true stress exceeds the polymer's tensile strength[42] or a craze initiation criterion,[78] the polymer will exhibit brittle fracture, indicating that polymer failure is always preceded by localized plastic deformation.

Although the deformation and aging kinetics are, as discussed before, essentially independent of molecular weight, the polymer's strength can be affected quite strongly.[79–82] As a result, changes in failure mode can be anticipated, albeit without an observable change in the kinetics involved.[1] Also in our work, an influence of molecular weight is perceived. The high molecular weight grade PC used in isothermal conditions exhibit ductile failure in contrast to the brittle failure that is observed for the low molecular weight grade PC in the mechanical domain of the nonisothermal experiments.

VI. Conclusions

A comprehensive investigation to failure of polycarbonate (PC) under cyclic fatigue loading has been performed. In a previous study we developed, and validated, a 3D constitutive model that is capable to predict the occurrence of plastic instabilities, yielding quantitative predictions of the lifetime of polycarbonate under *constant load*.[1] Here we demonstrated that the same approach is also applicable to predict the life span of polycarbonate under *cyclic loading* conditions (high cycle fatigue), over a large range of molecular weights and thermal histories, with a single parameter set only. First, an attempt was made to predict the fatigue life of PC under isothermal conditions. As for the case of constant stress, the model yields quantitative lifetime predictions under cyclic loading, both in uniaxial tension and uniaxial compression. It should be noted that the method is also applicable to other loading geometries as was demonstrated for static loading.[1] Essential for the prediction of an endurance limit is the implementation of aging kinetics that were shown to be accelerated by the cyclic stress applied. As a result of that stress, an increase in yield stress was observed and predicted.

Next, tests under nonisothermal conditions were investigated. In agreement with literature, failure could be subdivided into two domains: thermally and mechanically dominated failure. In the first domain, which is found at high stress, the (ductile) failure observed is caused by dissipative heating, as shown by infrared thermography. Large hysteresis loops were observed. In the second domain, which occurs at low stress, heating has no effect on failure. In between these two extremes usually a plateau is found, where the time-to-failure increases with 2 decades (see Figure 9). The changeover stress at which this plateau is located is highly dependent on (dissipative) heating, and therefore, it is expected that parameters like the size of the sample (surface area to volume ratio) affect this critical stress. In correspondence to the aging observed, as reflected in the increase in yield stress during fatigue loading, the presence of a ductile-to-brittle transition between the two domains is a second indication for physical aging to take place during testing. Finally, a rather abrupt decrease in energy dissipation per cycle is found at stresses below the critical changeover stress.

In order to perform quantitative fatigue life predictions under the more realistic, nonisothermal conditions found in practice, a thermomechanically coupled approach is required. It is essential that the constitutive model used in the numerical computations provides a realistic description of the energy dissipated per cycle. It was shown that the single mode approximation of the currently employed 3D elasto-viscoplastic model used for solid polymers is inadequate to capture energy dissipation. An extension of the current single-mode approximation to a simplified multimode description of the behavior up to yield was shown to be successful to predict the temperature rise in linear fatigue loading. Thus, to perform simulations of nonisothermal fatigue loading up to failure, the full constitutive equation has to be improved similarly with a multiple-mode description that covers the viscoelastic part. This work is currently being done in our group.[77]

Acknowledgment. The authors acknowledge the financial support provided by the Dutch Polymer Institute (DPI Project 445).

Appendix. The Retardation Time Spectrum

The retardation time spectrum determined by Klompen[72] is reproduced in Table 3. The values of this spectrum are obtained from experiments on Lexan161R samples with an S_a value of 28.3. The Lexan101R samples used in this study have an S_a value of 29.5. For that reason, the original time spectrum is shifted according to eq 20, giving the values in Table 4 used in this study.

References and Notes

(1) Klompen, E. T. J.; Engels, T. A. P.; van Breemen, L. C. A.; Schreurs, P. J. G.; Govaert, L. E.; Meijer, H. E. H. *Macromolecules* **2005**, *38*, 7009–7017.
(2) Stewart, R. *Plast. Eng.* **2005**, *61*, 18–28.
(3) Sakai, M.; Tateno, Y.; Arai, K.; Morioka, K. US Patent 5,722,295, 1998.
(4) Kurokawa, M.; Uchiyama, Y.; Nagai, S. *Tribol. Int.* **1999**, *32*, 491–497.
(5) Kurokawa, M.; Uchiyama, Y.; Nagai, S. *Wear* **2003**, *254*, 468–473.
(6) Brown, R. P. *Rapra Rev. Rep.* **2001**, *12*, 135.
(7) Zaheed, L.; Jachuck, R. J. *J. Appl. Therm. Eng.* **2004**, *24*, 2323–2358.
(8) Beardmore, P.; Rabinowitz, S. Fatigue deformation in polymers. In *Plastic Deformation of Materials: Treatise on Materials Science and Technology*; Arsenault, R. J., Ed.; Academic Press: New York, 1975.
(9) Hertzberg, R. W.; Manson, J. A. *Fatigue of Engineering Plastics*; Academic Press: New York, 1980.
(10) Sauer, J. A.; Richardson, G. C. *Int. J. Fract.* **1980**, *16*, 499–532.
(11) Gotham, K. V. *Dev. Plast. Technol.* **1986**, *16*, 155–201.
(12) Lesser, A. J. *Encycl. Polym. Sci. Technol.* **2002**, *6*, 197–251.
(13) Riddel, M. N.; Koo, G. P.; O'Toole, J. L. *Polym. Eng. Sci.* **1966**, *6*, 363–368.
(14) Constable, I.; Williams, J. G.; Burns, D. J. *J. Mech. Eng. Sci.* **1970**, *12*, 20–29.
(15) Crawford, R. J.; Benham, P. P. *J. Mater. Sci.* **1974**, *9*, 18–28.
(16) Crawford, R. J.; Benham, P. P. *Polymer* **1974**, *16*, 908–914.
(17) Sauer, J. A.; Foden, E.; Morrow, D. R. *Polym. Eng. Sci.* **1977**, *17*, 246–250.
(18) Rittel, D. *Mech. Mater.* **2000**, *32*, 131–147.
(19) Tauchert, T. R. *Int. J. Eng. Sci.* **1967**, *5*, 353–365.
(20) Tauchert, T. R.; Afzal, S. M. *J. Appl. Phys.* **1967**, *38*, 4568–4572.
(21) Justice, L. A.; Schultz, J. M. *J. Mater. Sci. Lett.* **1980**, *15*, 1584–1585.
(22) Lesser, A. J. *J. Appl. Polym. Sci.* **1995**, *58*, 869–879.
(23) Takahara, A.; Yamada, K.; Kajiyama, T.; Takayanagi, M. *J. Appl. Polym. Sci.* **1980**, *25*, 597–614.
(24) Takahara, A.; Yamada, K.; Kajiyama, T.; Takayanagi, M. *J. Appl. Polym. Sci.* **1981**, *26*, 1085–1104.
(25) Gotham, K. V. *Plast. Polym.* **1969**, *37*, 309–319.
(26) Crawford, R. J.; Benham, P. P. *J. Mech. Eng. Sci.* **1974**, *16*, 178–191.
(27) Jones, N. A.; Lesser, A. J. *J. Polym. Sci., Polym. Phys. Ed.* **1998**, *36*, 2751–2760.
(28) Szocs, F.; Klimová, M. *Eur. Polym. J.* **1996**, *32*, 1087–1089.
(29) Szocs, F.; Klimová, M.; Bartos, J. *Polym. Degrad. Stab.* **1997**, *55*, 233–235.
(30) Zilvar, V. *Plast. Polym.* **1971**, *39*, 328–332.
(31) Bouda, V.; Zilvar, V.; Staverman, J. A. *J. Polym. Sci., Polym. Phys. Ed.* **1976**, *14*, 2313–2323.
(32) Klompen, E. T. J.; Engels, T. A. P.; Govaert, L. E.; Meijer, H. E. H. *Macromolecules* **2005**, *38*, 6997–7008.
(33) Sternstein, S. S. *Polym. Prepr.* **1976**, *17*, 136–141.
(34) Nanzai, Y.; Miwa, A.; Cui, S. Z. *Polym. J.* **2000**, *32*, 51–56.
(35) Nanzai, Y.; Cui, S. Z. *Polym. J.* **2001**, *33*, 444–449.
(36) Li, X.; Yee, A. F.; Gidley, D. W. *J. Polym. Sci., Part B: Polym. Phys.* **1992**, *30*, 221–230.
(37) Bouda, V. *Polym. Bull.* **1982**, *7*, 639–644.
(38) LeGrand, D. G. *J. Appl. Polym. Sci.* **1969**, *13*, 2129–2147.
(39) Bubeck, R. A.; Bales, S. E.; Lee, H.-D. *Polym. Eng. Sci.* **1984**, *24*, 1142–1148.
(40) Hill, A. J.; Heater, K. J.; Agrawal, C. M. *J. Polym. Sci., Part B: Polym. Phys.* **1990**, *28*, 387–405.
(41) Arnold, J. C. *Polym. Eng. Sci.* **1995**, *35*, 165–169.
(42) van Melick, H. G. H.; Govaert, L. E.; Meijer, H. E. H. *Polymer* **2003**, *44*, 3579–3591.
(43) Govaert, L. E.; Timmermans, P. J. G.; Brekelmans, W. A. M. *J. Eng. Mater. Technol.* **2000**, *122*, 177–185.
(44) Li, X.; Hristov, H. A.; Yee, A. F.; Gidley, D. W. *Polymer* **1995**, *36*, 759–765.
(45) Dixon, S. R.; Hill, A. J.; O'Donnell, J. A. *Polym. Degrad. Stab.* **2005**, *89*, 208–219.
(46) Arad, S.; Radon, J. C.; Culver, L. E. *Polym. Eng. Sci.* **1972**, *12*, 193–198.
(47) Williams, J. G. *J. Mater. Sci.* **1977**, *12*, 2525–2533.
(48) Pitman, G.; Ward, I. M. *J. Mater. Sci.* **1980**, *15*, 635–645.
(49) Wyzgoski, M. G.; Novak, G. E. *J. Mater. Sci.* **2005**, *40*, 295–308.
(50) Sauer, J. A.; Chen, C. C. *Adv. Polym. Sci.* **1983**, *52–3*, 169–224.
(51) Jansssen, R. P. M.; Govaert, L. E.; Meijer, *Macromolecules* **2008**, *41*, 2531–2540.
(52) Coleman, B. D. *J. Polym. Sci.* **1956**, *20*, 447–455.
(53) Regel, V. R.; Leksovsky, A. M. *Int. J. Fract.* **1967**, *3*, 99–109.
(54) McKenna, G. B.; Penn, R. W. *Polymer* **1980**, *21*, 213–220.
(55) Engels, T. A. P.; Govaert, L. E.; Peters, G. W. M.; Meijer, H. E. H. *Proc. 13th Int. Conf. Deformation, Yield Fracture Polym.* **2006**, 69–72.
(56) Govaert, L. E.; Engels, T. A. P.; Klompen, E. T. J.; Peters, G. W. M.; Meijer, H. E. H. *Int. Polym. Process.* **2005**, *XX* (2), 170–177.
(57) Engels, T. A. P.; Govaert, L. E.; Peters, G. W. M.; Meijer, H. E. H. *J. Polym. Sci., Part B: Polym. Phys.* **2006**, *44*, 1212–1225.
(58) Koenen, J. A. *Polymer* **1992**, *33*, 4732–4736.
(59) Haward, R.; Thackray, G. *Proc. R. Soc. London A* **1968**, *302*, 453–472.
(60) Duckett, R. A.; Goswami, B. C.; Smith, L. S. A.; Ward, I. M.; Zihlif, A. M. *Br. Polym. J* **1978**, *10*, 11–16.
(61) Macosko, C. W. *Rheology; Principles, Measurements, and Applications*; VCH Publishers: New York, 1994.
(62) Bauwens-Crowet, C.; Bauwens, J.-C. *Polymer* **1982**, *23*, 1599–1604.
(63) Hasan, O. A.; Boyce, M. C.; Li, X. S.; Berko, S. *J. Polym. Sci., Part B: Polym. Phys.* **1993**, *31*, 185–197.
(64) Ho, C. H.; Vu-Khanh, T. *Polymer* **2003**, *23*, 1599–1604.
(65) Bauwens-Crowet, C.; Bauwens, J.-C. *Polymer* **1990**, *31*, 248–252.
(66) Bauwens-Crowet, C.; Bauwens, J.-C. *Polymer* **1990**, *31*, 646–650.
(67) Othmezouri-Decerf, J. *Polymer* **1994**, *35*, 4734–4742.
(68) Othmezouri-Decerf, J. *J. Mater. Sci.* **1999**, *34*, 2351–2359.
(69) Yang, Y.; D'Amore, A.; Di, Y.; Nicolais, L.; Li, B. *J. Appl. Polym. Sci.* **1999**, *59*, 1159–1166.
(70) van Melick, H. G. H.; Govaert, L. E.; Meijer, H. E. H. *Polymer* **2003**, *44*, 457–465.
(71) Rittel, D.; Rabin, Y. *Mech. Mater.* **2000**, *32*, 149–159.
(72) Klompen, E. T. J. PhD Thesis, Materials Technology, Eindhoven University of Technology, 2005.
(73) Maher, J. W.; Haward, R. N.; Hay, J. N. *J. Polym. Sci., Part B: Polym. Phys.* **1980**, *18*, 2169–2179.
(74) Adams, G. W.; Farris, R. J. *J. Polym. Sci., Part B: Polym. Phys.* **1988**, *26*, 433–445.
(75) Rittel, D. *Mech. Mater.* **1999**, *31*, 131–139.
(76) Li, Z.; Lambros, J. *Int. J. Solids Struct.* **2001**, *38*, 3549–3562.
(77) van Breemen, L. C. A.; den Hartog, M.; Govaert, L. E.; Meijer, H. E. H., manuscript in progress.
(78) van Melick, H. G. H.; Bresser, O. F. J. T.; den Toonder, J. M. J.; Govaert, L. E.; Meijer, H. E. H. *Polymer* **2003**, *44*, 2481–2491.
(79) Flory, P. J. *J. Am. Chem. Soc.* **1945**, *67*, 2048–2050.
(80) Vincent, P. I. *Polymer* **1960**, *1*, 425–444.
(81) Gent, A. W.; Thomas, A. G. *J. Polym. Sci., Part A2* **1972**, *10*, 571–573.
(82) Bersted, B. H.; Anderson, T. G. *J. Appl. Polym. Sci.* **1990**, *39*, 499–514.

MA071273I